

High harmonic optomechanical oscillations in the lithium niobate photonic crystal nanocavity

Cite as: Appl. Phys. Lett. **117**, 081102 (2020); <https://doi.org/10.1063/5.0016334>

Submitted: 04 June 2020 . Accepted: 17 August 2020 . Published Online: 25 August 2020

Haowei Jiang, Xiongshuo Yan, Hanxiao Liang, Rui Luo , Xianfeng Chen, Yuping Chen , and Qiang Lin 



View Online



Export Citation



CrossMark

ARTICLES YOU MAY BE INTERESTED IN

[Anisotropic domains and antiferrodistortive-transition controlled magnetization in epitaxial manganite films on vicinal SrTiO₃ substrates](#)

Applied Physics Letters **117**, 081903 (2020); <https://doi.org/10.1063/5.0016371>

[Lithium-niobate-on-insulator waveguide-integrated superconducting nanowire single-photon detectors](#)

Applied Physics Letters **116**, 151102 (2020); <https://doi.org/10.1063/1.5142852>

[Incorporation of erbium ions into thin-film lithium niobate integrated photonics](#)

Applied Physics Letters **116**, 151103 (2020); <https://doi.org/10.1063/1.5142631>

Lock-in Amplifiers
up to 600 MHz



Watch



High harmonic optomechanical oscillations in the lithium niobate photonic crystal nanocavity

Cite as: Appl. Phys. Lett. **117**, 081102 (2020); doi: [10.1063/5.0016334](https://doi.org/10.1063/5.0016334)

Submitted: 4 June 2020 · Accepted: 17 August 2020 ·

Published Online: 25 August 2020






View Online



Export Citation



CrossMark

Haowei Jiang,¹ Xiongshuo Yan,¹ Hanxiao Liang,² Rui Luo,³  Xianfeng Chen,¹ Yuping Chen,^{1,a)} 
and Qiang Lin^{2,b)} 

AFFILIATIONS

¹State Key Laboratory of Advanced Optical Communication Systems and Networks, School of Physics and Astronomy, Shanghai Jiao Tong University, Shanghai 200240, China

²Department of Electrical and Computer Engineering, University of Rochester, Rochester, New York 14627, USA

³Institute of Optics, University of Rochester, Rochester, New York 14627, USA

^{a)}Author to whom correspondence should be addressed: ypchen@sjtu.edu.cn

^{b)}Electronic mail: qiang.lin@rochester.edu

ABSTRACT

We explore the optomechanical coupling in an on-chip lithium niobate (LN) photonic crystal nanocavity. A mechanical frequency shift and nonlinear mechanical oscillations are observed with the intracavity power increasing. A 14th harmonic oscillation is generated at the intracavity power of $430 \mu\text{W}$ in the LN photonic crystal, which potentially can function as a mechanical frequency comb. The photonic crystal structure also shows the positive temperature coefficient of frequency, while the LN crystal has a negative intrinsic temperature coefficient. These characters of optomechanics in LN may play important roles in photon-phonon coupling or detector systems such as sensitive displacement and the mass and force detection.

Published under license by AIP Publishing. <https://doi.org/10.1063/5.0016334>

Lithium niobate (LN) has been widely studied and applied in the past few decades.^{1–3} Thanks to its rich properties, lithium niobate has been used to demonstrate many on-chip optical devices. Efficient photon-pair source⁴ and frequency doubler^{5,6} are designed relying on its high nonlinear coefficient. Benefiting from the high electro-optic coefficient, lithium niobate modulators^{7,8} have even been commercially used. Photonic crystal nanocavities exhibit superior capability of confining light in sub-wavelength dimension and, thus, are of great promise for light-matter interactions.^{9–12} Recently, we have developed high-quality one-dimensional photonic crystal nanobeam resonators on the LN platform,¹³ with optical Q up to $\sim 10^5$ while maintaining a small effective mode volume of $\sim (\frac{\lambda}{n})^3$. In this paper, we utilize this type of device to demonstrate nonlinear optomechanical oscillations in the lithium niobate photonic crystal nanobeam.

Cavity optomechanics has shown to be an attractive field exploring the interaction between optical signals and mechanical motions.¹⁴ The radiation pressure, raised up from the momentum transfer of photons and known as optical tweezers, has performed well in trapping dielectric particles.¹⁵ What is more, quite a few of applications based on optomechanics have been demonstrated these recent years,

such as microcavity cooling,¹⁶ bio-sensing with cavity optomechanical spring,¹⁷ and sensitive displacement sensors.¹⁸

Here, we present the measured optomechanics properties in a LN photonic crystal nanocavity. With the intracavity power of the LN device increasing, not only the mechanical resonance shifts and heats up but also harmonic oscillations up to 14th order are observed in the LN photonic crystal nanocavity.

The one-dimensional photonic crystal nanocavity with a $40 \mu\text{m}$ length [Fig. 1(a)] was fabricated on a 300 nm X-cut congruent LN-on-insulator (LNOI) wafer. The structure is patterned using electron beam lithography with ZEP-520A positive resist and etched by argon-ion milling. The buried silica layer between the LN nanobeam and the silicon substrate is finally undercut by diluted hydrofluoric acid to form a suspended photonic crystal nanocavity. The inset of Fig. 1(a) is the top view of two unit cells of the device. The LN photonic crystal nanocavity has dimensions of the width $w = 750 \text{ nm}$ and a lattice constant of 545 nm. It has a thickness of 250 nm, with a $2\text{-}\mu\text{m}$ gap from the silicon substrate. More details about the device design and fabrication can be found in our previous literature.¹³

In the LN photonic crystal nanocavity, considering the under-coupled condition, the optical mode transmission $T(\lambda)$ is modified by

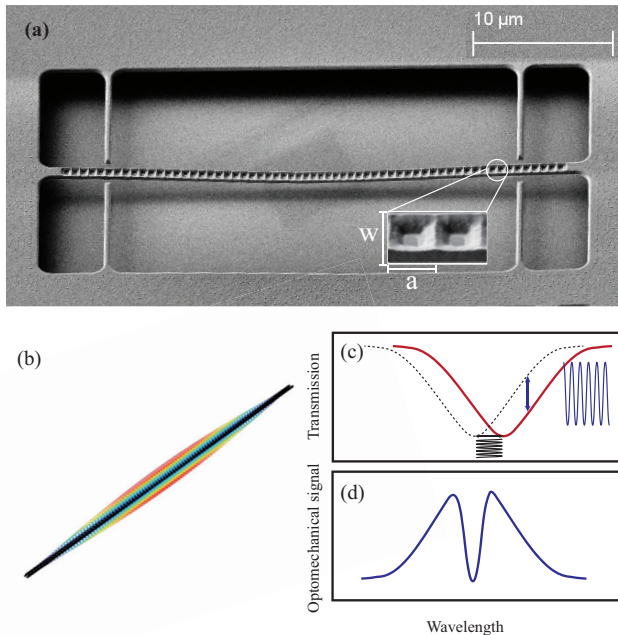


FIG. 1. (a) Scanning electron micrograph (SEM) of the photonic crystal nanocavity. Inset: two unit cells of the device with dimensions of $w = 750$ nm and lattice constant $a = 545$ nm. (b) Displacement fields of dispersive coupling of the device modes. (c) Changes of dispersive and dissipative coupling of the resonance line shape, respectively. (d) Amplitude of the optomechanical signal almost goes to zero at peak point.

the shift of the mechanical resonator position dx , as the following equation:¹⁹

$$dT = \left(g_{OM} \frac{\partial T}{\partial \omega_0} + g_e \frac{\partial T}{\partial \gamma_e} \right) dx. \quad (1)$$

The mechanical motion dx of the nanobeam cavity can modulate the external photon decay rate γ_e into the coupling taper fiber, with the external dissipative coupling coefficient of $g_e = d\gamma_e/dx$. The optical force can also raise up the other mechanical motion that modifies the nanocavity size, resulting in a dispersive coupling to the cavity frequency ω_0 , with a coupling coefficient of $g_{OM} = d\omega_0/dx$. Here, we notice that the dissipative optomechanical signal depends linearly on the unipolar parameter of $|\partial T/\partial \gamma_e|$, and the dispersive optomechanical signal is in a linear relationship with the bipolar parameter of $|\partial T/\partial \omega_0|$. The two couplings have different power density spectra. In the case of dissipative coupling, the maximum power density can be obtained at the center of the optical mode. However, a valley can be observed in mechanical power spectral density at the center wavelength of the optical mode for the dispersive mode [Figs. 1(b)–1(d)].

Figure 2 shows the schematic of the experimental setup, where a tunable continuous-wave laser (New Focus TLB-8800) is used as a light source. 1% of the laser is split into a Mach-Zehnder interferometer to calibrate the optical frequency detuning. 99% of the laser followed by a variable optical attenuator (VOA) and polarization controller (PC) then launched into a tapered and dimpled optical fiber to couple light into and out of the LNOI device. 5% of the output

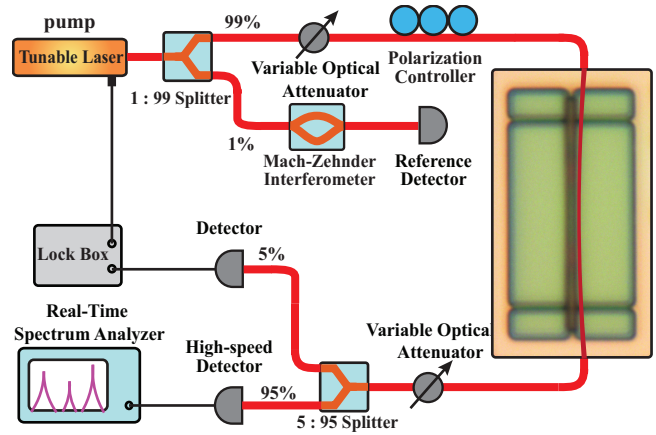


FIG. 2. Schematic of the experimental setup.

power from the LNOI device supplies a feedback to the lock box and helps stabilize the laser. The major part of the laser launched into device raises up an optomechanical coupling, and a set of mechanical modes are encouraged and can be observed from the real-time spectrum analyzer. In addition, the LN chip was placed on a thermoelectric cooler (TEC) with a fixed temperature set at 27 °C. The temperature of the TEC was stabilized by a temperature controller to prevent the temperature induced drifting of the device.

To identify the optomechanical coupling, we need to select a proper intracavity power, which is enough to excite a measurable mechanical mode and not too high to lock the laser at both sides of the optical mode. In our experiment, with the highest intracavity power at the mode center about 8 μW, the optical transmission and the power spectral density curve can be achieved [Figs. 3(a) and 3(b)]. It is worth stating that uneven wavelength sampling of Fig. 3(b) is just because of the limited laser accuracy that we can control. A valley is clearly located at the center of the power density curve, corresponding to the same wavelength of the center of the optical mode.

The device used in this work has an optical mode at the wavelength of 1504.7 nm, with a Q-factor of 6.29×10^4 [Fig. 3(c)]. Excluding the background spectrum that already has some radio frequency signals without intracavity power in the LN device, the strongest mechanical signal is at the frequency of 1.7 MHz, which turns out to come from a dispersive coupling. The intrinsic quality factor of the 1.7 MHz mechanical mode is 65.38 in the air environment [Fig. 3(d)]. We will concentratedly study around the 1.7 MHz mechanical mode in this paper.

To characterize the power dependence of the optomechanical oscillation, still we lock the laser halfway down on the blue side of the optical resonance. Figure 4 shows the mechanical frequency and measured power, dependence with the intracavity power varying in a large range from 4.3 μW to 430 μW. The mechanical resonance experiences a linear frequency shift in Fig. 4(a), with the power rising up, at a rate of about 625 Hz/μW. As shown in Fig. 4(b), the mechanical mode power density increases slowly with the intracavity power before 100 μW. After that, it experiences a strong heating up with the intracavity power increasing. However, something interesting happens:

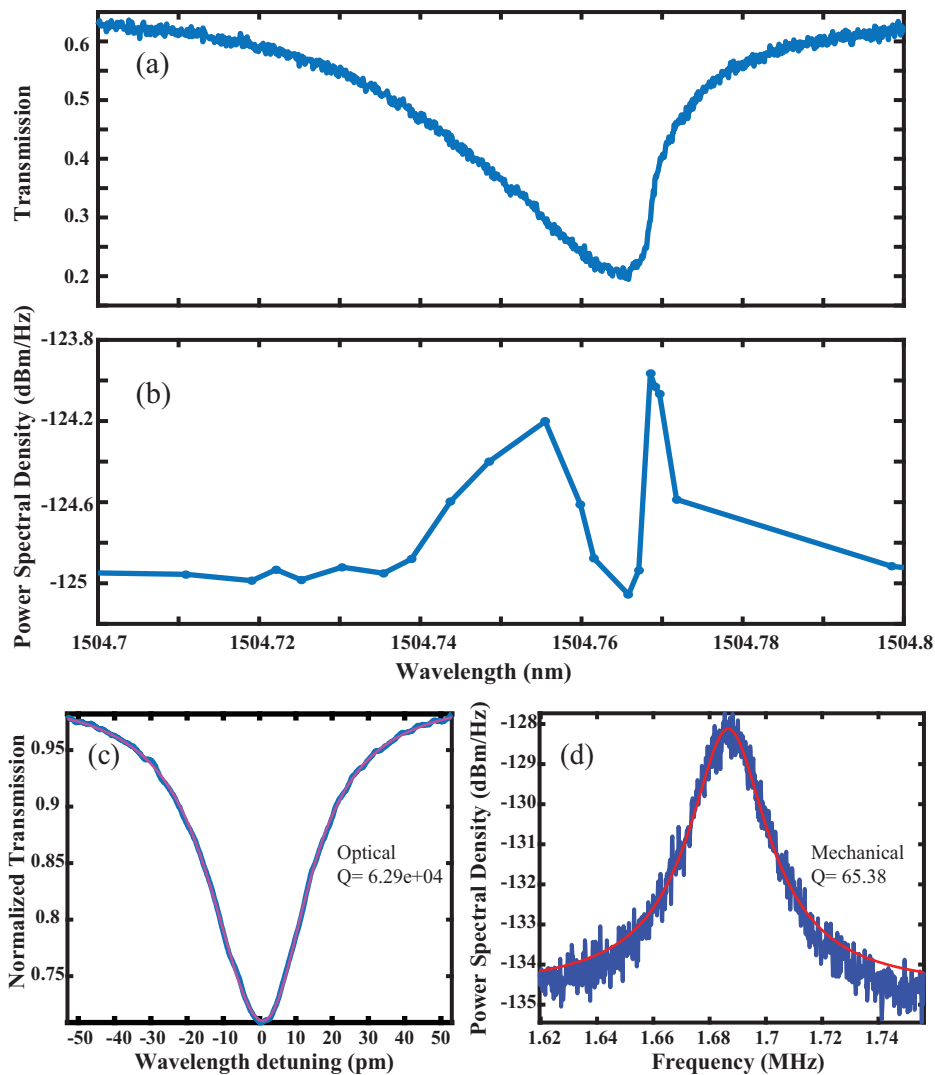


FIG. 3. (a) Transmission of the optical mode with the highest intracavity power about $8 \mu\text{W}$. (b) The power spectral density change with the wavelength for the 1.7 MHz mechanical mode. (c) Optical mode with a Q factor of 6.29×10^4 at the wavelength of 1504.7 nm. (d) Mechanical mode with a Q factor of 65.38.

when the intracavity power comes to $150 \mu\text{W}$, the mechanical power density slows down. The mechanical mode increasing stopped after $220 \mu\text{W}$, and a slow dropping down can even be observed when the intracavity power goes on increasing. Until now, we mainly focus on characterizing the dispersive coupling induced mechanical resonance at the frequency of about 1.7 MHz. The saturation of the mechanical model intensity after $220 \mu\text{W}$ seems it does not meet the principle of energy conservation, which means that the extra applied energy must have gone to somewhere else.

To figure out what happened to the nanocavity after $150 \mu\text{W}$, we check the mechanical frequency from 0 to 8 GHz. Comparing the distribution of modes with the intracavity power below and above $150 \mu\text{W}$, the major difference appears at the frequency of 40 MHz (Fig. 5). In Fig. 5, the intracavity powers of blue, red, orange, and purple curves are $0 \mu\text{W}$, $43 \mu\text{W}$, $136 \mu\text{W}$, and $430 \mu\text{W}$, respectively. There are some additional small peaks shown as the first curves are environmental noise. To characterize detailedly the

difference in mechanical oscillation, we set the spanning range from 0.5 MHz to 29.5 MHz and take more detailed power dependent data as shown the inset figure in Fig. 5. In Fig. 5, the first peak from the left is the fundamental mechanical mode, which has the same intensity trend as shown in Fig. 4(b). The second peak with a twice frequency is a second harmonic oscillation signal. At most, a 14th harmonic oscillation at the frequency of about 27.2 MHz is observed in testing. The mechanical harmonic generation turns out to be a step-by-step process. The fundamental oscillation heating up process slows down at around $150 \mu\text{W}$, and the 2nd harmonic mode arises at the same time. Then with the power going up, the third, fourth, and more harmonic mode arise one-by-one, which is similar to a “nonlinear mechanical oscillator.”²⁰ In the low intracavity power condition, the radiation-pressure arising from the momentum transfer of photons cannot show the obvious high oscillations, and then it is hard to measure it. With the intracavity power increasing and exceeding a certain value ($220 \mu\text{W}$ in

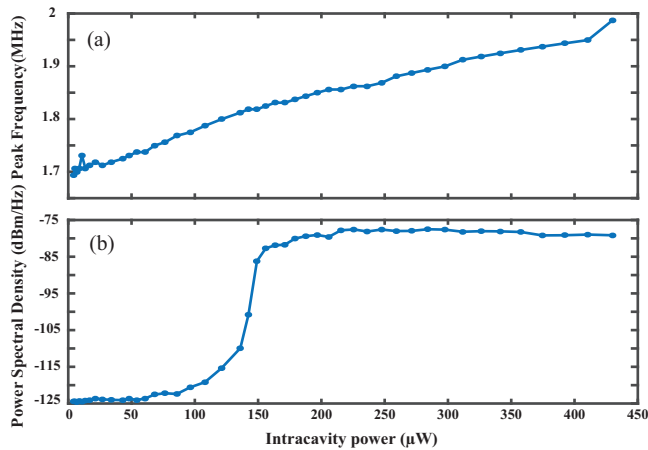


FIG. 4. Power dependence of the optomechanical oscillation. (a) Mechanical frequency shifts and (b) Mechanical mode intensity changes with the intracavity power increasing from $4.3 \mu\text{W}$ to $430 \mu\text{W}$.

our experiment), more energy can be coupled into the high oscillations and then the 14th harmonic oscillation can be observed.

In addition, the device is found experiencing differently with temperature changing. To characterize the temperature dependence of the device, the TEC's temperature setting is accurately modified by the temperature controller. The temperature scanning range is from 19.5°C to 27.5°C , by the step of 0.5°C . The tunable laser is locked halfway down on the blue side of the optical mode, and the intracavity power is fixed at $21.5 \mu\text{W}$. Figure 6 shows the mechanical spectra obtained from a Real-time spectrum analyzer (RSA) with different temperature settings. It tells that the mechanical mode intensity does not show a change while the mode frequency experiences a continuous shift with the temperature increasing. The mechanical frequency of the nanocavity shows a positive temperature coefficient, at a rate of $30 \text{ kHz}/^\circ\text{C}$, which is equivalent to a rate of about $2\%/^\circ\text{C}$. We know

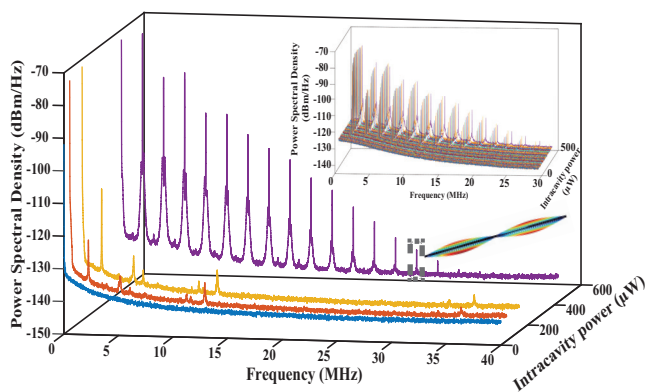


FIG. 5. Frequency spectrum obtained from the real-time spectrum analyzer, with the frequency range of 0–40 MHz. The intracavity powers of blue, red, orange, and purple curves are $0 \mu\text{W}$, $43 \mu\text{W}$, $136 \mu\text{W}$, and $430 \mu\text{W}$, respectively. The inset upper figure shows that the more detailed high harmonic optomechanical oscillations observed in the LN device. The bottom inset shows the mechanical displacement profile of the labeled mode (27.2 MHz), simulated by the finite element method.

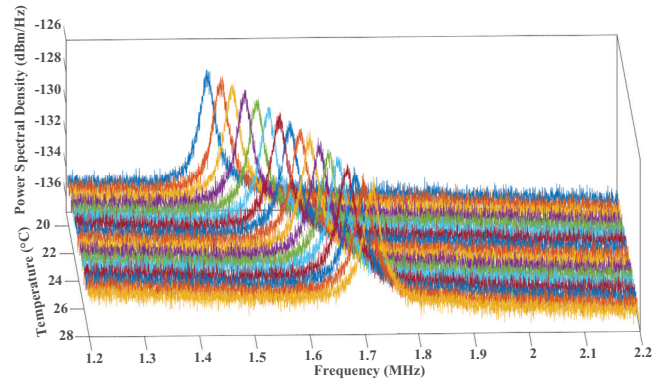


FIG. 6. Temperature dependence of the optomechanical coupling with the intracavity power of $21.5 \mu\text{W}$. The temperature varies from 19.5°C to 27.5°C .

that bulk LN would become mechanically soft with an increasing temperature because of the negative correlation between the stiffness constant and the temperature. Therefore, the mechanical mode frequency may decrease with the temperature increasing. However, there are different cases for our device on the LNOI. Thin film SiO_2 in the LNOI can be used to compensate the relative temperature dependence of the stiffness constant of LN, which can make the positive temperature coefficient of frequency (TCF).²¹ We think that is one of the main reasons that we can observe the mechanical frequency has a strong positive response to temperature in our device. Although our photonic crystal nanobeam is suspended, the other region of the LN thin film is involved in the thin film SiO_2 .

In conclusion, the optomechanical coupling in the photonic crystal nanocavity introduces interesting phenomena. While characterizing the power dependence, we noticed that the mechanical mode heating up slows down after a specific power. Nonlinear mechanical oscillations are generated after the specific power, and at most a 14th harmonic oscillation is observed in our experiment. A strong positive temperature dependence is achieved around room temperature. The LN photonic crystal nanocavity turns out to be a good platform for the potential sensitive displacement sensing, the temperature-to-mechanical sensing, or the nonlinear mechanical oscillation generator, which may function as a mechanical frequency comb.

AUTHORS' CONTRIBUTIONS

H.J. and X.Y. contributed equally to this work.

This work was supported by the National Key R & D Program of China (Nos. 2019YFB2203500 and 2017YFA0303700), the National Natural Science Foundation of China (NSFC) (Nos. 91950107 and 11574208), and the National Science Foundation (NSF) (Nos. ECCS-1810169 and ECCS-1842691). It was performed in part at the Cornell NanoScale Facility, a member of the National Nanotechnology Coordinated Infrastructure (NNCI).

DATA AVAILABILITY

The data that support the findings of this study are available from the corresponding author upon reasonable request.

REFERENCES

- ¹R. Weis and T. Gaylord, "Lithium niobate: Summary of physical properties and crystal structure," *Appl. Phys. A* **37**, 191–203 (1985).
- ²D. H. Jundt, "Temperature-dependent sellmeier equation for the index of refraction, n_e , in congruent lithium niobate," *Opt. Lett.* **22**, 1553–1555 (1997).
- ³H. Jiang, R. Luo, H. Liang, X. Chen, Y. Chen, and Q. Lin, "Fast response of photorefraction in lithium niobate microresonators," *Opt. Lett.* **42**, 3267–3270 (2017).
- ⁴S. Tanzilli, H. De Riedmatten, W. Tittel, H. Zbinden, P. Baldi, M. De Micheli, D. B. Ostrowsky, and N. Gisin, "Highly efficient photon-pair source using periodically poled lithium niobate waveguide," *Electron. Lett.* **37**, 26–28 (2001).
- ⁵G. Miller, R. Batchko, W. Tulloch, D. Weise, M. Fejer, and R. Byer, "42%-efficient single-pass CW second-harmonic generation in periodically poled lithium niobate," *Opt. Lett.* **22**, 1834–1836 (1997).
- ⁶L. Ge, Y. Chen, H. Jiang, G. Li, B. Zhu, Y. Liu, and X. Chen, "Broadband quasi-phase matching in a MgO:PPLN thin film," *Photonics Res.* **6**, 954–958 (2018).
- ⁷C. Wang, M. Zhang, X. Chen, M. Bertrand, A. Shams-Ansari, S. Chandrasekhar, P. Winzer, and M. Lončar, "Integrated lithium niobate electro-optic modulators operating at CMOS-compatible voltages," *Nature* **562**, 101 (2018).
- ⁸E. L. Wooten, K. M. Kissa, A. Yi-Yan, E. J. Murphy, D. A. Lafaw, P. F. Hallemeier, D. Maack, D. V. Attanasio, D. J. Fritz, G. J. McBrien *et al.*, "A review of lithium niobate modulators for fiber-optic communications systems," *IEEE J. Sel. Top. Quantum Electron.* **6**, 69–82 (2000).
- ⁹S. Noda, M. Fujita, and T. Asano, "Spontaneous-emission control by photonic crystals and nanocavities," *Nat. Photonics* **1**, 449 (2007).
- ¹⁰P. Lalanne, C. Sauvan, and J. P. Hugonin, "Photon confinement in photonic crystal nanocavities," *Laser Photonics Rev.* **2**, 514–526 (2008).
- ¹¹M. Notomi, "Manipulating light with strongly modulated photonic crystals," *Rep. Prog. Phys.* **73**, 096501 (2010).
- ¹²J. D. Joannopoulos, S. G. Johnson, J. N. Winn, and R. D. Meade, *Photonic Crystals: Molding the Flow of Light* (Princeton University Press, 2011).
- ¹³H. Liang, R. Luo, Y. He, H. Jiang, and Q. Lin, "High-quality lithium niobate photonic crystal nanocavities," *Optica* **4**, 1251–1258 (2017).
- ¹⁴T. J. Kippenberg and K. J. Vahala, "Cavity optomechanics: Back-action at the mesoscale," *Science* **321**, 1172–1176 (2008).
- ¹⁵D. G. Grier, "A revolution in optical manipulation," *Nature* **424**, 810 (2003).
- ¹⁶O. Arcizet, P.-F. Cohadon, T. Briant, M. Pinard, and A. Heidmann, "Radiation-pressure cooling and optomechanical instability of a micromirror," *Nature* **444**, 71–75 (2006).
- ¹⁷W. Yu, W. C. Jiang, Q. Lin, and T. Lu, "Cavity optomechanical spring sensing of single molecules," *Nat. Commun.* **7**, 12311 (2016).
- ¹⁸H. Miao, K. Srinivasan, and V. Aksyuk, "A microelectromechanically controlled cavity optomechanical sensing system," *New J. Phys.* **14**, 075015 (2012).
- ¹⁹M. Wu, A. C. Hryciw, C. Healey, D. P. Lake, H. Jayakumar, M. R. Freeman, J. P. Davis, and P. E. Barclay, "Dissipative and dispersive optomechanics in a nanocavity torque sensor," *Phys. Rev. X* **4**, 021052 (2014).
- ²⁰V. I. Nekorkin, *Introduction to Nonlinear Oscillations* (John Wiley & Sons, 2015).
- ²¹L. Shi and G. Piazza, "Lithium niobate on silicon dioxide suspended membranes: A technology platform for engineering the temperature coefficient of frequency of high electromechanical coupling resonators," *J. Microelectromech. Syst.* **23**, 1318–1329 (2014).